AGU PUBLICATIONS

Geophysical Research Letters

RESEARCH LETTER
10.1002/2016GL072452

Key Points:
- Efficiency of turbulent mixing in the abyssal ocean is highly variable, as opposed to being considered a constant traditionally
- Variations in mixing efficiency has a leading order impact on the rate of overturning of the abyssal branch of circulation
- Abyssal ocean turbulence plays a leading role in regulating the ocean's role in the carbon cycle and likely other tracer budgets

Supporting Information:
- Supporting Information S1

Correspondence to:
A. Mashayek,
ali_mash@mit.edu

Citation:
Mashayek, A., H. Salehipour, D. Bouffard, C. P. Caulfield, R. Ferrari, M. Nikurashin, W. R. Peltier, and W. D. Smyth (2017), Efficiency of turbulent mixing in the abyssal ocean circulation, *Geophys. Res. Lett.*, *44*, 6296–6306, doi:10.1002/2016GL072452.

Received 25 DEC 2016
Accepted 26 APR 2017
Accepted article online 2 MAY 2017
Published online 22 JUN 2017

Efficiency of turbulent mixing in the abyssal ocean circulation

A. Mashayek[1], H. Salehipour[2], D. Bouffard[3], C. P. Caulfield[4], R. Ferrari[1], M. Nikurashin[5], W. R. Peltier[2], and W. D. Smyth[6]

[1]Department of Earth Atmosphere and Planetary Sciences, Massachusetts Institute of Technology, Cambridge, Massachusetts, USA, [2]Department of Physics, University of Toronto, Toronto, Ontario, Canada, [3]Surface Waters Research and Management, Eawag – Swiss Federal Institute of Aquatic Science and Technology, Kastanienbaum, Switzerland, [4]BP Institute and Department of Applied Mathematics and Theoretical Physics, University of Cambridge, Cambridge, UK, [5]Arc Centre of Excellence for Climate Science, Sydney, Australia; University of Tasmania, Hobart, Australia, [6]College of Earth Ocean and Atmospheric Sciences, Oregon State University, Corvallis, Oregon, USA

Abstract Turbulent mixing produced by breaking of internal waves plays an important role in setting the patterns of downwelling and upwelling of deep dense waters and thereby helps sustain the global deep ocean overturning circulation. A key parameter used to characterize turbulent mixing is its efficiency, defined here as the fraction of the energy available to turbulence that is invested in mixing. Efficiency is conventionally approximated by a constant value near one sixth. Here we show that efficiency varies significantly in the abyssal ocean and can be as large as approximately one third in density stratified regions near topographic features. Our results indicate that variations in efficiency exert a first-order control over the rate of overturning of the lower branch of the meridional overturning circulation.

1. Introduction

The meridional overturning circulation (MOC) of the ocean plays a primary role in the climate system through its role in the uptake, transport, and storage of heat and carbon in the ocean [*Hansen et al.*, 1985]. The strength of the abyssal branch of the overturning circulation is proportional to mixing, which enables deep dense waters formed at high latitudes to rise back toward the surface [*Ferrari*, 2014]. The mixing is primarily due to turbulence induced by breaking of internal gravity waves occurring away from ocean margins, but mainly around bottom topographic features. The waves are generated by barotropic tides or geostrophic eddies impinging upon bottom topographic features [*Garrett*, 2003; *Alford*, 2003; *Nikurashin and Ferrari*, 2013]. When internal waves break, energetic turbulence is produced and the density is "mixed," resulting in a vertical density flux (an effective vertical mass flux) because the turbulence develops in an ocean that is stably stratified in density. Close to the top and bottom boundaries, the nature of mixing changes from that induced by the internal wave breaking to boundary layer processes which control the density flux within a narrow boundary layer.

The spatial scales at which mixing occurs are orders of magnitude smaller than those resolved in numerical models of the global ocean circulation. Furthermore, direct measurements of turbulent buoyancy fluxes in the abyssal ocean are sparse for practical reasons and are nearly absent within the bottom boundary layers. Hence, it is common to represent the collective effect of small-scale mixing of salinity, temperature, and tracers in terms of mixing coefficients, often referred to as cross-density (diapycnal) turbulent diffusivities which are several orders of magnitude larger than the corresponding molecular diffusion coefficients. The turbulent diffusion coefficient for buoyancy, κ, remains poorly constrained on a regional scale which leads to uncertainties in simulations of the deep ocean circulation; the rate of overturning associated with the abyssal branch of the MOC in numerical models is directly related to global patterns of mixing represented by spatially variable diffusivity in the models [*Munk and Wunsch*, 1998; *Large et al.*, 1994; *Mashayek et al.*, 2015]. A common method for obtaining an estimate of κ in the ocean interior (not in the boundary layer) from observations is to relate it to measurements of the rate of turbulent kinetic energy dissipation, ϵ, and stratification, N, through the relation [*Osborn*, 1980]:

$$\kappa = \Gamma \frac{\epsilon}{N^2} = \nu\, \Gamma \left[\frac{\epsilon}{\nu N^2}\right] = \nu\, \Gamma\, Re_b, \tag{1}$$

where ν is the kinematic viscosity of seawater. N is a measure of the density stratification, known as the buoyancy frequency which is defined as $N = \sqrt{(-g/\rho_0)\rho_z}$ where g is the acceleration due to gravity, ρ_0 is a reference density for seawater, and ρ_z is the vertical gradient of neutral density. Neutral density is a variable that eliminates the dynamically irrelevant compressibility effects from the full density, an important correction in the weakly stratified abyssal ocean [*Jackett and McDougall*, 1997]. Γ is the flux coefficient defined as

$$\Gamma = \frac{\eta}{1-\eta}. \tag{2}$$

η is the mixing efficiency defined as the ratio of the rate of energy spent on irreversible mixing of different density waters ($\mathcal{M}$), to the total rate of energy available to turbulence which is the sum of $\mathcal{M}$ and the rate of energy dissipation to heat (ϵ). (see *Peltier and Caulfield*, 2003 for a review of the methodology that must be applied to determine $\mathcal{M}$ on the basis of a separation between reversible and irreversible mixing processes.) We note that Γ is often mistakenly referred to as an "efficiency" in the oceanographic community even though it can be larger (in fact much larger) than 1. We will refer to it by its original name "flux coefficient," noting that the two are interchangeable through (2). $Re_b = \epsilon/(\nu N^2)$, often referred to as the "buoyancy Reynolds number," represents the ratio of the tendency of turbulence to mix density vertically to the combined influence of stratification and viscosity in suppressing vertical motion and turbulence. Re_b is commonly understood to be a measure of turbulence "intensity." Equation (1) is widely used to estimate mixing rates in the ocean [see e.g., *Waterhouse et al.*, 2014] and in global climate models [*Jayne and Laurent*, 2001; *Polzin*, 2009].

Despite extensive evidence that Γ varies over a wide range in different geophysical environments [e.g., *Moum*, 1996; *Ruddick et al.*, 1997; *Smyth et al.*, 2001; *Mashayek and Peltier*, 2013; *Salehipour et al.*, 2016a] (see supporting information for a discussion), for practical reasons Γ has commonly been approximated by a constant equal to 0.2 (corresponding to $\eta = 1/6$) [*Wunsch and Ferrari*, 2004]. From a global budget perspective, Γ plays an important role, since it represents the fraction of energy available to the turbulent mixing that helps sustain the abyssal ocean circulation [*Wunsch and Ferrari*, 2004]. This leading order global impact is the focus of this work. Recent developments in both numerical simulation and field measurements have allowed us to develop a refined parameterization of Γ.

In a recent study, *De Lavergne et al.* [2016] investigated the role of a variable flux coefficient in determining the rate of circulation of the abyssal MOC. They argued that locally breaking internal waves are likely to be too rare or sparsely occurring to provide sufficient mixing to sustain an abyssal overturning rate of $\sim$15 Sv (1 Sv = 10^6 m^3/s), inferred from inverse methods that assimilate a variety of ocean data (to be discussed further in what follows). They concluded that additional processes ought to be responsible for providing the necessary upwelling required for closure of the abyssal MOC. Their analysis was based on the parameterization of *Shih et al.* [2005], as modified by *Bouffard and Boegman* [2013]. However, these parameterizations do not account for higher mixing efficiencies of 0.3–0.5 that have been reported in recent literature [*Mashayek and Peltier*, 2013; *Mashayek et al.*, 2013a; *Salehipour et al.*, 2015; *Chalamalla and Sarkar*, 2015]. In this study, we will demonstrate, based on our recent construction of an unprecedentedly large suite of direct numerical simulations (DNS), (i) that deep ocean mixing is likely significantly more efficient than assumed by *De Lavergne et al.*, 2016 and hence sufficiently strong, on its own, to provide the energy required for closure of the abyssal MOC and (ii) that spatial variability of Γ plays a key role in vertical patterns and exchanges between the abyssal and middepth branches of the global MOC.

We emphasize that this study does not cover the turbulence in the bottom boundary layer within which equation (1) does not necessarily hold and the definition of flux coefficient, in the conventional sense, might not hold. As discussed in *Ferrari et al.* [2016], insofar as the global MOC is concerned the value of the flux at the top of the bottom boundary layer is of concern. In our analysis we make the common assumption that such flux is set by enhanced internal wave breaking above rough topography. However, we note that understanding of the underlying physics of boundary turbulence and the extent to which it may affect the flux at the top of the boundary layer are coming to the forefront of ocean mixing discussions.

2. A Global Map of Abyssal Turbulence Intensity

Figure 1 (left) shows a global map of ϵ constructed on the basis of an extension of *Nikurashin and Ferrari* [2013] as discussed in *Ferrari et al.* [2016]. Their estimate of ϵ is based on the linear energy conversion from tidal and

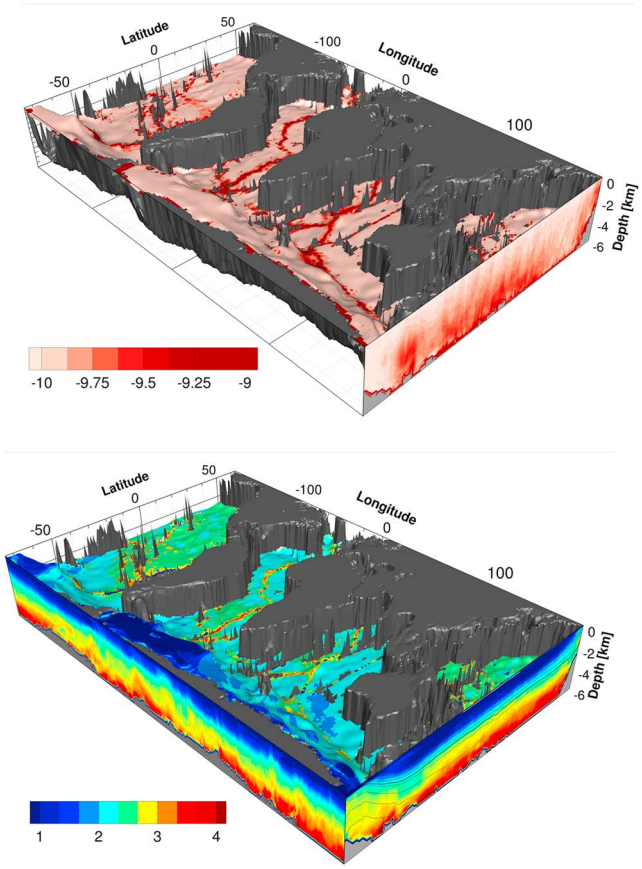

Figure 1. (top) Global map of rate of dissipation of kinetic energy, ϵ, plotted on the density surface $\gamma = 28$ kg/m^3 in the abyssal ocean. The right face shows the same quantity zonally averaged. (bottom) Map of buoyancy Reynolds number, Re_b as defined in (1), on the same density surface as in Figure 1 (top). The right and front surfaces show zonal and meridional averages. The black lines overlaid on the contour map on the right face show zonally averaged density from the World Ocean Circulation Experiment (WOCE). The thick black line represents the neutral density $\gamma = 28$ kg/m^3, which marks the boundary between density surfaces which ventilate at high latitudes in both hemispheres and those which only ventilate in the Southern Ocean. Both maps are constructed based on estimates of rate of dissipation of kinetic energy from *Nikurashin and Ferrari* [2013] and WOCE stratification.

geostrophic flows into internal waves above rough topography [*Nycander*, 2005; *Nikurashin and Ferrari*, 2011] combined with a parameterization for turbulent energy dissipation resulting from the breaking of internal waves generated by tidal flows over rough topography [*St Laurent et al.*, 2002]. Of particular importance to the research reported in this letter are two key assumptions which have a leading order impact on the global distribution of ϵ. First, it was assumed that the fraction of the radiated energy going into dissipation locally is ~30% based on observations, and that this local dissipation decays upward away from the ocean floor with a decay scale of 500 m. Second, the estimate of ϵ does not explicitly take into account the mixing induced by breaking of internal waves generated in the far field. This contribution is likely more important at middepths and, as will be discussed later, we take this somewhat into account by assuming that it results in a constant background interior mixing. In short, global estimates of ϵ are not available and it is for practical reasons that we rely on a distribution subject to the collectivity of these assumptions. Our focus is not upon the distribution of ϵ, however. We will simply employ this map to study the efficiency of mixing and show that it is of leading order importance for the oceanic bulk energy budget and closure of the abyssal MOC.

The turbulent dissipation rate, ϵ, in Figure 1 (left) corresponding to the neutral density surface $\gamma = 28$ kg/m^3 is plotted over this density level. This density level approximately marks the separation between the two counterrotating cells, an abyssal one and a middepth one, that characterize the MOC in a zonally averaged sense, and it comes to the surface only in the Southern Ocean [*Lumpkin and Speer*, 2007, see also Figure 4, top]. While the 28 kg/m^3 neutral density surface appears to divide the two branches of the MOC, this is just an

illusion of the zonal average. The two branches exchange waters as they flow between the Atlantic and Pacific Oceans. Our point here is that waters denser than 28 kg/m^3 are observed to rise from the abyss crossing density surfaces and must therefore become lighter as a result of mixing since there are no heating sources in the ocean interior. The zonally averaged global estimates of ϵ are illustrated on the right face of the domain box in Figure 1 (left) and show that ϵ is bottom enhanced in the vicinity of rough topographic features which are hot spots of wave generation and breaking consistent with observations as reviewed by *Waterhouse et al.* [2014].

The critical parameter which appears in the characterization of κ according to (1) is not ϵ but rather the ratio ϵ/N^2, as encapsulated in Re_b upon nondimensionalization by ν. Figure 1 (right) shows a global map of Re_b on the same isopycnal $\gamma = 28$ kg/m^3 along with its zonal and meridional averages on the side planes. (Both ϵ and N^2 are calculated on the vertical grid of the global hydrogaphy constructed based on WOCE; the vertical grid spacing changes from a few tens of meters at middepths to ~150 m in the deepest part of the ocean.) The density contours, shown by lines superimposed on the right face from a few, illustrate the stably stratified structure of a "pancake ocean" in which increasingly dense waters reside at increasing depth. Our focus is on density classes that outcrop only in the Southern Ocean, as they are associated with the abyssal branch of the MOC. The boundary between these isopycnals and those associated with the upper branch of the MOC, which outcrop in both hemispheres, is marked by a thick black line (i.e., $\gamma = 28$ kg/m^3).

Descending toward the ocean floor, $Re_b \propto \epsilon/N^2$ increases monotonically (Figure 1, right) as ϵ becomes enhanced and stratification weakens. Although an increase in Re_b implies a more intense level of turbulence, it does not necessarily lead to more efficient mixing. In the limit of weak stratification (small N), there is too little density contrast to be mixed. On the other hand, in the limit of overly strong turbulence (large ϵ), the stratification becomes irrelevant as most of the energy is lost to viscous dissipation and hence in heat production rather than being invested in mixing. Thus, by moving progressively farther into the abyss, it is expected that mixing efficiency (and hence Γ) should vary nonmonotonically despite the monotonic increase in Re_b. There must therefore exist a depth range in which an optimal balance of turbulence and stratification exists which allows for energetic turbulence to mix the moderate ambient stratification most efficiently.

3. The KH-ansatz: An "Idealized" Model Problem Useful for the Representation of Oceanic Turbulence

Recent progress, in both observational measurements and DNS analyses of stratified turbulence at sufficiently high Reynolds numbers, has led to a much improved understanding of the complex nature of oceanic turbulence and its associated mixing. A fundamental question nevertheless concerns the applicability or fidelity of such idealized DNS analyses as representative of actual mixing processes in the ocean. In particular, an idealized canonical model for the study of stratified turbulence is that based on a freely evolving stably stratified parallel shear flow that is susceptible to the emergence of a Kelvin-Helmholtz (KH) instability which subsequently collapses into turbulence (i.e., the "KH-ansatz"). Before we investigate the possible implications of this idealized model for abyssal ocean mixing, we must ensure that the KH-ansatz provides a plausible representation of mixing in the real ocean.

Figure 2 compares the variations of Γ with Re_b as inferred from the DNS data set as well as the observational oceanographic measurements. To assess carefully the fidelity of the KH-ansatz to ocean turbulence observations, we have distinguished between "young" and "mature" stages invoking the concept of turbulence "age." The young stage is associated with a growing and initially two dimensional KH billow which overturns the density interface and is characterized by rapid mixing of buoyancy but only weak dissipation of turbulent kinetic energy (hence, high mixing efficiencies). Turbulence becomes mature as soon as the billow collapses or the flow becomes fully three-dimensional, after which it begins to decay. In the observations, the age is assessed using the ratio of the Ozmidov and Thorpe length scales, following *Smyth et al.* [2001] (see the supporting information for further details [*Smyth and Moum*, 2012]).

The agreement between the KH-ansatz and the observations is compelling for both young and mature stages. Considering all of the idealizations employed in the DNS analyses and the assumptions involved in the observational estimates, it is encouraging that the KH-ansatz appears to represent the Re_b dependence of the oceanic flux coefficient for each stage quite accurately, (noting the histograms based on observational data on both the abscissa and ordinate of Figure 2). The DNS results for KH-ansatz turbulence associated with the

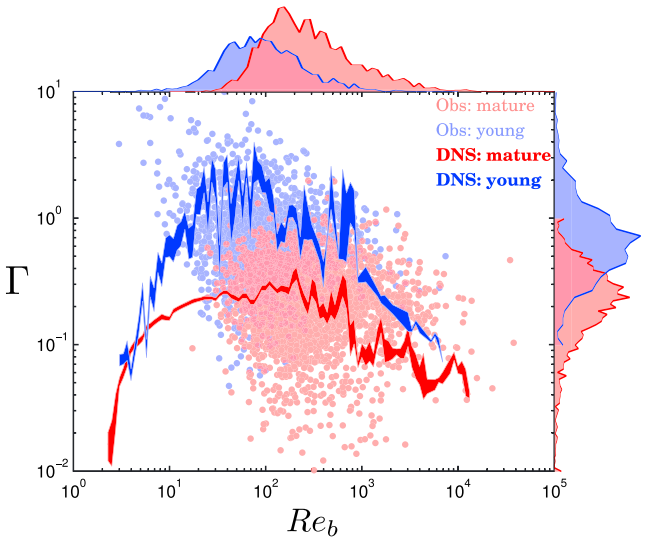

Figure 2. Re_b dependence of Γ, comparing the young and mature mixing events obtained from oceanic measurements of *Smyth et al.* [2001] (see *Moum* [1996] and *Lien et al.* [1995] for source of data) and an extensive suite of DNS analyses associated with the growth, turbulent breakdown, and decay of a Kelvin-Helmholtz instability (i.e., KH-ansatz) taken from *Salehipour and Peltier* [2015]. The histograms on both abscissa and ordinate illustrate the distribution of these mixing events in field observations. The DNS data sets are also binned for clarity of presentation.

mature stage have been employed by *Salehipour et al.* [2016a] to develop a parameterization that depends on other parameters in addition to Re_b.

It should be noted that the young overturns may be as important as the mature fully turbulent flows in their contribution to the overall diapycnal mixing. However, in contrast to the mature stage, whose mixing properties appear to be independent of the primary instability mechanism [see *Salehipour and Peltier*, 2015], the young overturns are inherently process dependent [*Salehipour et al.*, 2016b]. For this reason, and as in *Salehipour et al.* [2016a], we will employ the mature stage of the KH-ansatz as our idealized representation of oceanic turbulence. Although the contribution of young overturns is difficult to quantify, there is little doubt that its inclusion would increase the mixing efficiency (and hence Γ) of the ocean.

4. A Practical "Recipe" for the Flux Coefficient in the Deep Ocean

A more diverse set of observations as well as DNS data sets derived from KH-ansatz turbulence are employed in Figures 3a and 3b to illustrate the leading order variability of Γ with Re_b. The oceanic observations of *Smyth et al.* [2001] in Figure 3a are here a binned representation of the mature turbulence in their data set obtained from two different expeditions that have been jointly shown in Figure 2. Taken together, these panels reveal a nonmonotonic dependence of Γ on Re_b: $\Gamma \propto Re_b^{0.5}$ for $Re_b \ll Re_b^*$ where Re_b^* represents the peak Γ, and $\Gamma \propto Re_b^{-0.5}$ for $Re_b \gg Re_b^*$. The former scaling limit in the range of small to intermediate Re_b is consistent with previous observational, experimental, and numerical evidence as recently reviewed by *Bouffard and Boegman* [2013], whose data, shown in the figure, are also dominated by mature turbulence. For the right "flank" of the curve $\Gamma(Re_b)$, our data collectively support the scaling relation of $\Gamma \propto Re_b^{-0.5}$ as previously suggested based on DNS [*Shih et al.*, 2005] and observations [*Walter et al.*, 2014]. As a practical recipe we may join these two scaling regimes through a Padé approximant in the form

$$\Gamma(Re_b) = \frac{2\Gamma^* \left(\frac{Re_b}{Re_b^*}\right)^{\frac{1}{2}}}{1 + \left(\frac{Re_b}{Re_b^*}\right)}, \tag{3}$$

where Γ^* is the maximum value of the flux coefficient at $Re_b = Re_b^*$.

The two dashed curves in Figures 3a and 3b illustrate this parameterization with $(Re_b^*, \Gamma^*) = (100, 0.2)$ and (300,0.5) which enclose the upper and lower bounds on our collection of data and simulations in Figures 3a and 3b. This variability is associated with variations in parameters other than Re_b (for example, shear as represented by a bulk Richardson number; see the supporting information). The main goals of this study are to (a) explore the global implications of the nonmonotonic dependence of Γ on Re_b and (b) highlight the implications of the uncertainty enclosed within these lower and upper bounds for the impact of mixing on the MOC.

We note that Γ cannot be fully parameterized in terms of Re_b alone; it depends on other parameters [*Mashayek and Peltier*, 2013; *Mashayek et al.*, 2013a; *Salehipour et al.*, 2015, 2016a]. Our choice here is for practical reasons

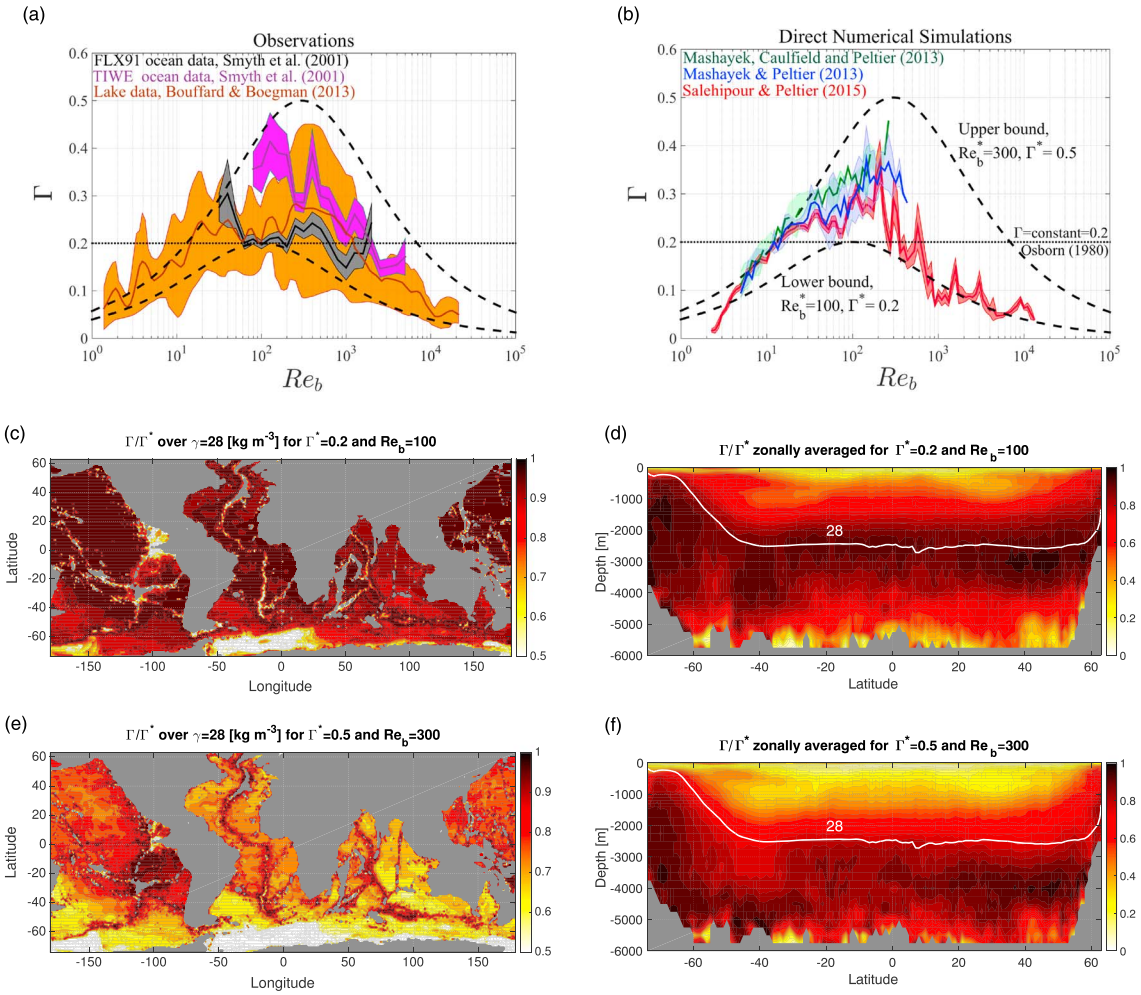

Figure 3. Re_b dependence of Γ as inferred from (a) various observational data sets and (b) DNS data sets (see supporting materials and *Winters et al.* [1995] and *Caulfield and Peltier* [2000] for details of quantification of mixing from DNS). The shadings, except for the orange curve in Figure 3a, illustrate the spread in data after binning (see supporting information for details). (c–f) Global maps of normalized flux coefficient Γ/Γ^* constructed based on the upper and lower bounds of Γ marked by dashed lines in the top panels. Figure 3c shows the global map on the abyssal density level 28 kg/m^3 corresponding to the lower bound curve with its globally zonally averaged Γ in Figure 3d. Figures 3e and 3f show the same for the upper bound curve. For reference, $\gamma = 28$ kg/m^3 surface is shown with a white line in Figures 3e and 3f.

since (a) those parameters are hard to identify over the global ocean and (b) the dependence of Γ upon them is still very much an active topic of research. Our focus is on the leading order impact of variations of Γ, parameterized in terms of a practical definition of the Reynolds number, on the deep ocean circulation.

5. Global Distribution of Γ in the Deep and Abyssal Ocean

Figures 3c–3f show maps of flux coefficient for the abyssal ocean. The maps correspond to the upper and lower bounds of Γ in Figure 3a and have been made by combining equation (3) with the three-dimensional map of Re_b in Figure 1 (right).

Based on the lower bound parameterization, Figures 3c and 3d suggest that Γ ~0.2 at middepths and becomes maximum about the interface between the upper and lower branches of the MOC, by the density level 28 kg/m^3. Γ is much smaller below the depth of 3500 m for this lower bound on the parameterization. For the upper bound parameterization, Figures 3e and 3f suggest that Γ is intensified in the abyssal ocean (to ~0.5) and is approximately half that value at intermediate depths that mark the upper limit of the abyssal branch of the MOC. In both maps, there exists a depth range in which the balance of ambient stratification and turbulence leads to optimal mixing. Γ decays to zero toward the ocean floor where stratification vanishes. The rate of abyssal circulation depends on turbulence intensity and stratification (the two being interconnected) and

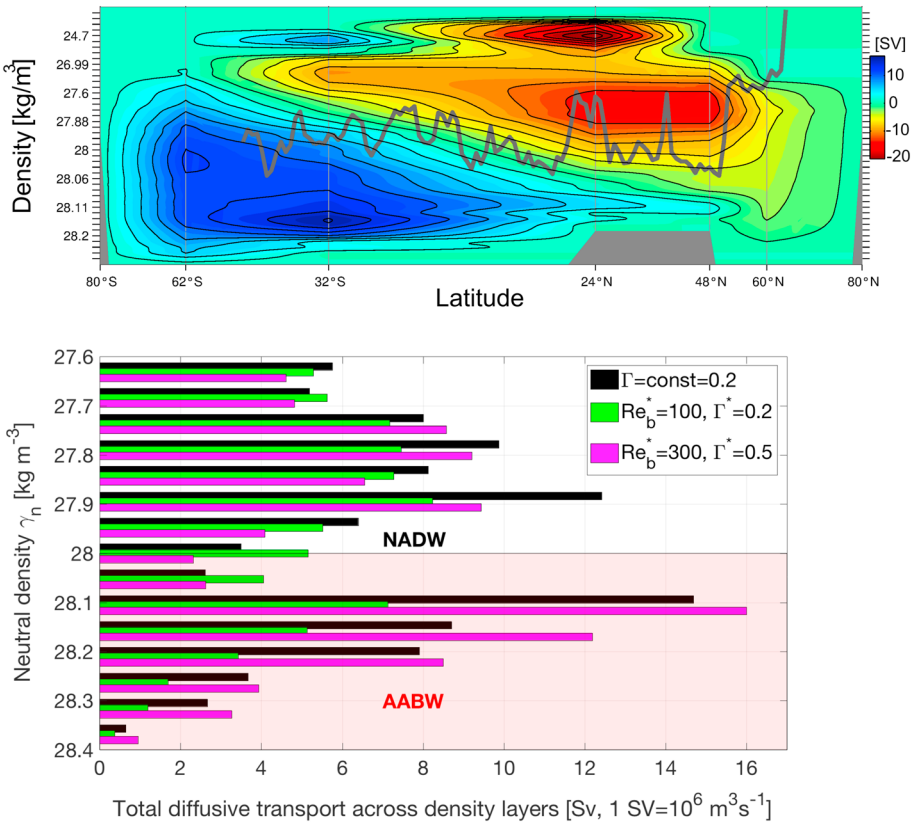

Figure 4. (top) Global zonally averaged meridional overturning circulation in Sverdrups (1 Sv=10^6 m^3/s), taken from *Lumpkin and Speer* [2007]. The blue and red streamlines indicate clockwise and counterclockwise overturning, respectively. The vertical axis represents neutral density which increases with ocean depth. While this figure is for a zonally and globally averaged streamline, the peak of the abyssal circulation is 12.4±2.6 Sv at 32°S in the Atlantic Ocean and 14.9±3.4 Sv at 32°S in the Pacific Ocean, while the net circumpolar circulation is 20.9±6.7 Sv at 32°S. (bottom) Estimates of rate of turbulent mixing across density surfaces, obtained based on a calculation similar to that of *Nikurashin and Ferrari* [2013] with three modifications as described in *Ferrari et al.* [2016] (see the supporting information for details). The calculation employs the Re_b map shown in Figure 1b and the two flux coefficient parameterization bounds of Figure 3a.

hence on Γ (as in (1)). Thus, when compared to a globally constant Γ, the lower bound maps (Figures 3c and 3d) imply a weaker abyssal ocean circulation while the upper bound maps (Figures 3e and 3f) imply a strong abyssal MOC. This may prove critical for setting the amount of carbon stored in the abyssal ocean, because the stronger the abyssal circulation, the faster deep carbon-rich waters come in contact with the surface and increase atmospheric CO_2.

In addition to the vertical variations in Γ (Figures 3d and 3f), its geographical distributions (Figures 3c and 3e) are also characterized by significant variability. The two parameterization limits differ in an important way: for the lower Γ bound (Figure 3c), there is anticorrelation between ϵ and Γ, while for the upper bound (Figure 3e) the correlation is positive. In other words, for the upper/lower bound, turbulence is most/least efficient at the depths where the abyssal MOC appears to be strongest.

6. Discussion

Figure 4(top) shows a decade-mean globally and zonally averaged ocean meridional overturning circulation from *Lumpkin and Speer* [2007] which was estimated using inverse techniques that incorporated air-sea fluxes of heat and freshwater, hydrographic sections, and current measurements. The ragged line represents the mean depth of ocean ridge crests. Mixing is enhanced and influential on the MOC below the crest of mid-ocean ridges, because the abyssal wavefield is radiated from topography and some of its energy gets converted to mixing due to wave breaking in the close vicinity of topography. Based on Figure 1 (right; rightmost face of the domain), the 28 kg/m^3 density class that marks the upper extent of the zonally averaged

abyssal MOC lies within the ragged line in Figure 4 (top), confirming that it is exposed to vigorous mixing and thus its strength must be sensitive to the value of mixing efficiency.

Figure 4 (bottom) shows the rate of transport of water masses across various density levels (i.e., across horizontal levels in Figure 4, top) calculated for $\Gamma = 0.2$ as well as for the upper and lower bounds of our parameterization of Γ (shown in Figures 3a and 3b). See the supporting information for a detailed discussion of the methodology employed to construct this figure. Since the estimate considers only the waves that break locally close to topography (i.e., only 30% conversion of energy into mixing plus dissipation), it does not take into account the contribution due to upward propagating waves which radiate away from topography (i.e., the other 70% of energy). As discussed by *Waterhouse et al.* [2014], in most regions, mixing is primarily due to the local internal wavefield while in a few cases (out of many oceanic data sets they compiled to study global patterns of mixing), the contribution due to remote internal wave sources becomes relevant. At most locations, they found that in the abyssal ocean the total power lost through turbulent dissipation is less than the input into the local internal wavefield, suggesting that the radiating energy is dissipated in the far field likely in shallow continental margins. Thus, we argue that our assumption of mixing due to locally generated turbulence is reasonable for this study which focuses on the abyssal branch of the MOC (within the shaded region in Figure 4, bottom). For lighter water classes, above the shaded region, we have added a constant background dissipation rate (based on the compilation of observations reported in *Waterhouse et al.* [2014]) to represent the interior mixing by the background radiating field.

The rate of overturning of the abyssal MOC cell is largest based on the upper bound parameterization of Γ, with the peak being ~20 Sv (1 Sv=10^6 m^3/s). This value lies within the low-intermediate range of the various observationally constrained estimates [*Ganachaud and Wunsch*, 2000; *Talley et al.*, 2003; *Lumpkin and Speer*, 2007; *Garabato et al.*, 2014]. More specifically, it is close to the mean value of 20.9 ± 6.7 Sv overturning according to *Lumpkin and Speer* [2007] and as reported in the caption of Figure 4 (top). The overturning rate obtained based on the lower bound parameterization of Γ, instead, falls short of the lower limit of this estimate (i.e., <14.2 Sv). The crucial point here is that the difference between the upper and lower bounds of Γ produces a leading order difference in the strength of the MOC, and hence, such variability needs to be considered in our assessments of the mixing-induced abyssal branch of ocean circulation.

From a globally averaged perspective, the constant flux coefficient of 0.2 (i.e., efficiency of one sixth) produces the same abyssal MOC strength as that produced by the upper bound parameterization of Γ. This fortuitous finding, despite being interesting, should not be construed to imply that the value of 0.2 is a robust estimate for the flux coefficient on different spatial or temporal scales (e.g., see Figures 3c and 3e for spatial distributions away from 0.2). Furthermore, there is no reason to assume a priori that an abyssal mean value of 0.2 is a property of the ocean under a variable climate.

As noted earlier, it has been suggested by *De Lavergne et al.* [2016] that mixing due to breaking of internal waves near rough bottom topography may be insufficient to explain the strength of the abyssal circulation inferred from inverse techniques. This would suggest that other processes are necessary to provide additional energy to sustain the abyssal MOC, with geothermal heat flux proposed as one candidate by earlier works [*Adcroft et al.*, 2001; *Emile-Geay and Madec*, 2009; *Mashayek et al.*, 2013b; *De Lavergne et al.*, 2016]. While *Waterhouse et al.* [2014] provided some evidence that the contribution to mixing from the remotely generated waves in the deepest density classes might not be significant in a global sense, the question regarding their share of mixing is still open. Furthermore, it has been suggested that turbulence within the stratified boundary layer above the ocean floor can contribute to considerable mixing which, in combination with lateral advection, enhances the net mixing in the ocean interior [*Armi*, 1978; *Garrett*, 1990; *Mashayek et al.*, 2017].

Our results presented in Figure 4b take the influence of the geothermal heat flux into account [*Davies and Davies*, 2010], thereby providing an additional ~4.5 Sv of transformation to what was reported in *Ferrari et al.* [2016]. They suggest that while the upper bound on Γ provides sufficient (if not excessive) mixing for maintaining the lower branch of circulation, the lower bound clearly comes significantly short of it. This implies that all or some of the above mentioned additional processes may be necessary to provide the rest of the required mixing. As a result, the conclusion of *De Lavergne et al.* [2016] concerning the necessity of incorporating the geothermal heat flux in order to improve the closure of the abyssal circulation appears to be unwarranted: while the role of the basal flux should not be ignored, at this stage it is well within the uncertainty window.

7. Caveats and Road Map

Our analyses relies on a number of assumptions whose validity is a topic of active research in the field of density stratified turbulence. Three of those assumptions are worth discussing in more detail.

First, we argue that the standard parameterization $\Gamma = 0.2$ can be improved upon by assuming a $\Gamma = \mathcal{F}(Re_b)$ functional relationship. In fact, Γ has dependence upon other parameters. Such dependence is the topic of active research, likely of higher-order importance, and difficult to account for in a global scale calculation. Our focus was on exploring the nonmonotonic dependence of Γ on Re_b on the large-scale ocean circulation. We note that a more comprehensive parameterization of Γ was introduced in *Canuto et al.* [2010].

Second, we argue that the mature phase of KH turbulence, as computed via DNS, is a good model for ocean turbulence. The high mixing efficiency of very young billows in DNS results from the exceptionally sharp density interface that develops in the braid region between adjacent billows. In the real ocean, the persistent, compressive strain that sharpens that interface [*Smyth*, 1999] is scrambled by ambient small-scale turbulence, slowing the diffusion of mass across the interface and therefore reducing Γ. While we cannot yet quantify this effect, it is clear that it makes the young phase more like the mature phase.

Third, we further assume that the coevolution of instantaneous $\Gamma_i(t)$ and $Re_b(t)$ in decaying KH turbulence provides a good model for our hypothetical function $\Gamma = \mathcal{F}(Re_b)$. While our study provides some preliminary evidence in support of this, it will be subject to future confirmation as we explain below.

The above mentioned assumptions are open to question, but together they allow us a glimpse of the effect that improved Γ parameterizations will have on estimates of global ocean circulation. Variations in efficiency of mixing are of leading order importance for the ocean bulk energy budget and circulation and hence should be included in ocean and climate models.

In future work, of the above assumptions will be relaxed as follows. Our first assumption can be relaxed by including other parameters, such as Richardson number (*Ri*; see supporting information), as is pursued in ongoing work. Establishing the fluid dynamical basis of such dependence, while challenging on its own, has led to some recent progress, but a global estimate of *Ri* is not practically feasible at the moment. Regarding our second assumption, evidence to date suggests that the highly efficient young phase contributes one fourth to one third of net mixing. Rather than include the young phase explicitly (which would greatly complicate the parameterization problem), we recognize that our estimates are conservative and suggest that larger values of Γ are plausible. And finally, our third assumption can be relaxed by using Γ_{net}, a Γ defined as the integral over the whole life cycle of individual turbulent events, in place of Γ_i [e.g., *Smyth et al.*, 2001]. Due to the significant computational cost associated with the DNS data provided herein, this will require many more (time-consuming) simulations. This third assumption allows us to make progress in the very short term.

8. Summary

By comparison to ocean and lake measurements, we have verified the fidelity of the KH-ansatz as an appropriate model for the study of the mixing properties of oceanic turbulence. Based on a diverse set of direct numerical simulations and field measurements, we have proposed two bounding curves as parameterizations for Γ that describe its nonmonotonic dependence on Re_b. These two curves imply significantly different global distributions for abyssal ocean mixing, which in turn lead to substantial differences in the overturning strength at various isopycnal levels. Crucially, we have demonstrated that turbulent mixing due to bottom enhanced internal wave breaking can range anywhere from being fully capable of producing the overturning rate necessary for closure of the abyssal MOC to coming significantly short of it.

We emphasize that our focus is upon abyssal mixing above the bottom boundary layer. Understanding of variations of density flux within the boundary layer and across its interface with the overlying internal wave-induced mixing zone is of leading order importance and is rapidly evolving [*Ferrari et al.*, 2016; *Mashayek et al.*, 2017]. We expect such understanding, once sufficiently mature to be extended to the global ocean and to be complementary to this study. In the meantime, our parameterization provides a physical mechanism through which the effective buoyancy flux can tend towards zero within the well-mixed boundary layers in which stratification becomes vanishingly small. Of particular interest will be the variation of flux coefficient from the ocean interior, in which mixing is primarily induced by internal waves to the boundary layers in which

other physical processes induce a turbulent buoyancy flux. Within such boundary layers the flux transitions from that in the interior to the geothermal flux at the ocean floor.

A primary goal of the climate community over the past several decades has been to quantify the ability of the abyssal ocean to sequester carbon. Such storage partly depends on the residence time of carbon in the abyssal MOC cell, which in turn depends on both the rate of overturning and the rate of turbulent exchange of tracers between the abyssal and middepth MOC cells. Our study demonstrates that variations in Γ exert a leading order influence upon the rate of abyssal MOC.

Acknowledgments
We wish to thank Jim Moum, Mike Gregg, and Eric D'Asaro for stimulating discussions (not implying agreement with all our arguments). We are grateful to Jim Moum for sharing the data used in the construction of Figure 3a. A.M. acknowledges an NSERC PDF award. A.M. and R.F. acknowledge support from the U.S. National Science Foundation grant OCE-1233832. The research activity of C.P.C. is supported by the EPSRC Programme grant EP/K034529/1 entitled "Mathematical Underpinnings of Stratified Turbulence." The research of W.R.P. at Toronto is supported by NSERC Discovery grant A9627. M.N. acknowledges Australian Research Council Support through grant DE 150100937. The participation of W.D.S. was funded by the U.S. National Science Foundation under grants OCE-1030772 and OCE-1537173. The data used to construct Figures 1, 3, and 4 (bottom) are available at https://doi.org/10.17863/CAM.9452.

References

Adcroft, A., J. R. Scott, and J. Marotzke (2001), Impact of geothermal heating on the global ocean circulation, *Geophys. Res. Lett.*, *28*(9), 1735–1738.
Alford, M. H. (2003), Redistribution of energy available for ocean mixing by long-range propagation of internal waves, *Nature*, *423*(6936), 159–162.
Armi, L. (1978), Some evidence for boundary mixing in the deep ocean, *J. Geophys. Res.*, *83*(C4), 1971–1979.
Bouffard, D., and L. Boegman (2013), A diapycnal diffusivity model for stratified environmental flows, *Dyn. Atmos. Oceans*, *61*, 14–34.
Canuto, V. M., A. M. Howard, Y. Cheng, C. J. Muller, A. Leboissetier, and S. R. Jayne (2010), Ocean turbulence, III: New GISS vertical mixing scheme, *Ocean Modell.*, *34*(3), 70–91.
Caulfield, C., and W. Peltier (2000), Anatomy of the mixing transition in homogeneous and stratified free shear layers, *J. Fluid Mech.*, *413*, 1–47.
Chalamalla, V. K., and S. Sarkar (2015), Mixing, dissipation rate, and their overturn-based estimates in a near-bottom turbulent flow driven by internal tides, *J. Phys. Oceanogr.*, *45*(8), 1969–1987.
Davies, J. H., and D. R. Davies (2010), Earth's surface heat flux, *Solid Earth*, *1*(1), 5–24.
De Lavergne, C., G. Madec, J. Le Sommer, A. G. Nurser, and A. C. Naveira Garabato (2016), The impact of a variable mixing efficiency on the abyssal overturning, *J. Phys. Oceanogr.*, *46*(2), 663–681.
Emile-Geay, J., and G. Madec (2009), Geothermal heating, diapycnal mixing and the abyssal circulation, *Ocean Sci.*, *5*, 203–218.
Ferrari, R. (2014), Oceanography: What goes down must come up, *Nature*, *513*(7517), 179–180.
Ferrari, R., A. Mashayek, T. J. McDougall, M. Nikurashin, and J.-M. Campin (2016), Turning ocean mixing upside down, *J. Phys. Oceanogr.*, *46*, 2239–2261.
Ganachaud, A., and C. Wunsch (2000), Improved estimates of global ocean circulation, heat transport and mixing from hydrographic data, *Nature*, *408*(6811), 453–457.
Garabato, A. C. N., A. P. Williams, and S. Bacon (2014), The three-dimensional overturning circulation of the southern ocean during the WOCE era, *Prog. Oceanogr.*, *120*, 41–78.
Garrett, C. (1990), The role of secondary circulation in boundary mixing, *J. Geophys. Res.*, *95*(C3), 3181–3188.
Garrett, C. (2003), Internal tides and ocean mixing, *Science*, *301*(5641), 1858–1859.
Hansen, J., G. Russell, A. Lacis, I. Fung, D. Rind, and P. Stone (1985), Climate response times: Dependence on climate sensitivity and ocean mixing, *Science*, *229*(4716), 857–859.
Jackett, D., and T. McDougall (1997), A neutral density variable for the world's oceans, *J. Phys. Oceanogr.*, *27*(2), 237–263.
Jayne, S., and L. S. Laurent (2001), Parameterizing tidal dissipation over rough topography, *Geophys. Res. Lett.*, *28*, 811–814.
Large, W. G., J. C. McWilliams, and S. C. Doney (1994), Oceanic vertical mixing: A review and a model with a nonlocal boundary layer parameterization, *Rev. Geophys.*, *32*(4), 363–403.
Lien, R.-C., D. R. Caldwell, M. Gregg, and J. N. Moum (1995), Turbulence variability at the equator in the central Pacific at the beginning of the 1991–1993 El Niño, *J. Geophys. Res.*, *100*(C4), 6881–6898.
Lumpkin, R., and K. Speer (2007), Global ocean meridional overturning, *J. Phys. Oceanogr.*, *37*(10), 2550–2562.
Mashayek, A., and W. Peltier (2013), Shear-induced mixing in geophysical flows: Does the route to turbulence matter to its efficiency?, *J. Fluid Mech.*, *725*, 216–261.
Mashayek, A., C. Caulfield, and W. Peltier (2013a), Time-dependent, non-monotonic mixing in stratified turbulent shear flows: Implications for oceanographic estimates of buoyancy flux, *J. Fluid Mech.*, *736*, 570–593.
Mashayek, A., R. Ferrari, G. Vettoretti, and W. Peltier (2013b), The role of the geothermal heat flux in driving the abyssal ocean circulation, *Geophys. Res. Lett.*, *40*, 3144–3149, doi:10.1002/grl.50640.
Mashayek, A., R. Ferrari, M. Nikurashin, and W. Peltier (2015), Influence of enhanced abyssal diapycnal mixing on stratification and the ocean overturning circulation, *J. Phys. Oceanogr.*, *45*(10), 2580–2597.
Mashayek, A., F. Ferrari, S. Merrifield, J. Ledwell, L. St. Laurent, and A. Naveira Garabato (2017), Topographic enhancement of vertical turbulent mixing in the Southern Ocean, *Nature Commun.*, *8*, 14197.
Moum, J. (1996), Efficiency of mixing in the main thermocline, *101*(C5), 12,057–12,069.
Munk, W. H., and C. Wunsch (1998), Abyssal recipes II: Energetics of tidal and wind mixing, *Deep Sea Res.*, *45*, 1977–2010.
Nikurashin, M., and R. Ferrari (2011), Global energy conversion rate from geostrophic flows into internal lee waves in the deep ocean, *Geophys. Res. Lett.*, *38*, L08610, doi:10.1029/2011GL046576.
Nikurashin, M., and R. Ferrari (2013), Overturning circulation driven by breaking internal waves, *Geophys. Res.*, *40*, 3133–3137, doi:10.1002/grl.50542.
Nycander, J. (2005), Generation of internal waves in the deep ocean by tides, *J. Geophys. Res.*, *110*, C10028, doi:10.1029/2004JC002487.
Osborn, T. R. (1980), Estimates of the local rate of vertical diffusion from dissipation measurements, *J. Phys. Oceanogr.*, *10*, 83–89.
Peltier, W., and C. Caulfield (2003), Mixing efficiency in stratified shear flows, *Annu. Rev. Fluid Mech.*, *35*, 135–167.
Polzin, K. L. (2009), An abyssal recipe, *Ocean Modell.*, *30*(4), 298–309.
Ruddick, B., D. Walsh, and N. Oakey (1997), Variations in apparent mixing efficiency in the North Atlantic Central Water, *J. Phys. Oceanogr.*, *27*, 2589–2605.
Salehipour, H., and W. R. Peltier (2015), Diapycnal diffusivity, turbulent Prandtl number and mixing efficiency in Boussinesq stratified turbulence, *J. Fluid Mech.*, *775*, 464–500.
Salehipour, H., W. R. Peltier, and A. Mashayek (2015), Turbulent diapycnal mixing in stratified shear flows: The influence of Prandtl number on mixing efficiency and transition at high Reynolds number, *J. Fluid Mech.*, *773*, 178–223.

Salehipour, H., W. Peltier, C. Whalen, and J. MacKinnon (2016a), A new characterization of the turbulent diapycnal diffusivities of mass and momentum in the ocean, *Geophys. Res. Lett.*, *43*, 3370–3379, doi:10.1002/2016GL068184.

Salehipour, H., C. Caulfield, and W. Peltier (2016b), Turbulent mixing due to the Holmboe wave instability at high Reynolds number, *J. Fluid Mech.*, *803*, 591–621.

Shih, L. H., J. R. Koseff, G. N. Ivey, and J. H. Ferziger (2005), Parameterization of turbulent fluxes and scales using homogeneous sheared stably stratified turbulence simulations, *J. Fluid Mech.*, *525*, 193–214.

Smyth, W. (1999), Dissipation range geometry and scalar spectra in sheared, stratified turbulence, *J. Fluid Mech.*, *401*, 209–242.

Smyth, W., and J. Moum (2012), Ocean mixing by Kelvin-Helmholtz instability, *Oceanography*, *25*, 140–149.

Smyth, W., J. Moum, and D. Caldwell (2001), The efficiency of mixing in turbulent patches: Inferences from direct simulations and microstructure observations, *J. Phys. Oceanogr.*, *31*, 1969–1992.

St Laurent, L., H. Simmons, and S. Jayne (2002), Estimating tidally driven mixing in the deep ocean, *Geophys. Res. Lett.*, *29*(23), 2106, doi:10.1029/2002GL015633.

Talley, L. D., J. L. Reid, and P. E. Robbins (2003), Data-based meridional overturning streamfunctions for the global ocean, *J. Clim.*, *16*(19), 3213–3226.

Walter, R., M. Squibb, C. Woodson, J. Koseff, and S. Monismith (2014), Stratified turbulence in the nearshore coastal ocean: Dynamics and evolution in the presence of internal bores, *J. Geophys. Res. Oceans*, *119*, 8709–8730, doi:10.1002/2014JC010396.

Waterhouse, A. F., et al. (2014), Global patterns of diapycnal mixing from measurements of the turbulent dissipation rate, *J. Phys. Oceanogr.*, *44*, 1854–1872.

Winters, K., P. Lombard, J. Riley, and E. D'Asaro (1995), Available potential energy and mixing in density-stratified fluids, *J. Fluid Mech.*, *289*, 115–128.

Wunsch, C., and R. Ferrari (2004), Vertical mixing, energy, and the general circulation of the oceans, *Annu. Rev. Fluid Mech.*, *36*, 281–314.